Macromolecules

Article

Cite This: Macromolecules 2018, 51, 3059−3065

Capillary Imbibition of Polymer Mixtures in Nanopores

Yang Yao,[†] Hans-Juergen Butt,[†] Jiajia Zhou,[*,‡,§] Masao Doi,[§,∥] and George Floudas[*,†,⊥]

[†]Max Planck Institute for Polymer Research, 55128 Mainz, Germany

[‡]School of Chemistry, Key Lab Bioinspired Smart Interfacial Science & Technology of Ministry of Education, [§]Center of Soft Matter Physics and Its Applications, and [∥]Beijing Advanced Innovation Center for Biomedical Engineering, Beihang University, Beijing 100191, China

[⊥]Department of Physics, University of Ioannina, 45110 Ioannina, Greece

Supporting Information

ABSTRACT: Capillary imbibition of homogeneous mixtures of entangled poly(ethylene oxide) melts in nanopores of self-ordered nanoporous alumina follows a $t^{1/2}$ dependence but contradicts the classical Lucas−Washburn equation. Herein we employ reflection microscopy and self-consistent field theory (SCFT) calculations to demonstrate the *faster* penetration of nanopores for the *shorter* chains. Combined results suggest on average an ∼15% enrichment by the shorter chains. On top of that, SCFT shows an enrichment of the short chains near the pore surface. Possible applications in separating long and short polymer chains by the difference in imbibition speed—in the absence of solvent—are discussed.

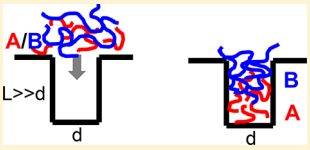

1. INTRODUCTION

Squeezing a polymer chain in a thin tube can have several applications in fields such as membranes, gel chromatography, oil recovery, etc.[1] Of particular interest is the case of a confining medium with sizes comparable to the molecular length scale. This is the case, for example, that the building blocks of life, i.e., DNA and proteins, are experiencing when migrating through a narrow passage with profound importance in cell biology.[2,3] When a polymer melt gets into contact with the opening of a thin pore, the capillary force is strong and drags the chains into the pore. Recent experiments, however, have shown that capillary imbibition of polymer melts into narrow pores is anything but trivial.[4−6] Capillary penetration of a series of entangled poly(ethylene oxide) (PEO) melts within nanopores of self-ordered alumina followed an approximate $t^{1/2}$ behavior according to the classical Lucas−Washburn equation (LWE); t is time.[7,8] However, a reversal in dynamics of capillary rise has been reported with increasing polymer molecular weight.[6] Chains with 50 entanglements or less show a slower capillary rise than theoretically predicted as opposed to chains with more entanglements that display a faster capillary rise.

Insight into the imbibition process of polymer melts can be obtained by studying polymer blends. Here we study capillary imbibition in polymer mixtures consisting of short and long chains of the same polymer. By employing both experiment and self-consistent field theory (SCFT) calculations, we demonstrate that in a binary mixture composed of long and short chains of the same chemical identity shorter chains penetrate consistently faster in narrow pores. By careful selection of the polymer molecular weights relative to the pore diameter, this procedure could be used in separating chains in a bimodal or polydisperse polymer melt in the absence of solvent.

2. EXPERIMENTAL SECTION

Sample Preparation. Poly(ethylene oxide)s (PEOs) with molecular weights of 50k (M_w = 53 090 g/mol, M_n = 44 510 g/mol) and 500k (M_w = 480 000 g/mol and M_n = 398 000 g/mol) and their mixtures were employed (PEO 50k, synthesis by Wagner and Thiel (MPI-P); PEO 500K purchased from Polymer Standards Service). Both homopolymers were synthesized via anionic polymerization with *tert*-butyl ether and hydroxyl end groups. For the mixtures, homopolymers with different mass fractions (75/25, 50/50, and 25/75) were dissolved in chloroform at a 10% polymer concentration. The solution was stirred for 24 h to ensure uniform mixing. Subsequently, the solvent was allowed to evaporate at ambient temperature for 5 days followed by heating at 90 °C for 3 days to completely remove any traces of solvent. As for the nanopores, we employ self-ordered nanoporous aluminum oxide (AAO) that contains arrays of discrete-isolated, parallel cylindrical nanopores that are uniform in length and diameter. AAO templates with pore depth of 100 μm and pore diameters of 65 and 25 nm were prepared following methods reported in the literature.[9−11]

Method of Imbibition. Polymer films were hot-pressed (100 μm) at 100 °C and placed above the AAO template at a fixed distance maintained by PEO pillars (diameter 1 mm; length 2 mm). The temperature during the imbibition process was measured inside the vacuum oven by a thermometer located near the sample. The pillars were made of PEO (M_w = 5 × 10^3 g/mol) and kept the nanopores open during the application of vacuum. The oven was subsequently brought to 85 °C, i.e., some 15 °C above the equilibrium melting temperature of PEO. Melting of the pillars occurs at 62 °C while heating the oven to 85 °C takes ∼1.5 min. As the pillars melted, the polymer film got smoothly into contact with the AAO surface. Subsequently, the polymer melt was infiltrated into the nanopores under capillary force, and the imbibition process was monitored for specific time intervals. Following imbibition, the vacuum was purged with air, and the samples were quenched to room temperature. It takes ∼15 s for the polymer melt to crystallize. Then the sample was put in a fridge at −26 °C for 3 h to make sure the sample inside nanopores are crystalline (the homogeneous nucleation temperature of PEO of 50k inside AAO pores is around −16 °C). The estimated time corresponding to the complete freezing of the polymer in nanopores following imbibition is ∼20 s. This brings an uncertainty in the actual

Received: December 22, 2017
Revised: February 27, 2018
Published: April 9, 2018

DOI: 10.1021/acs.macromol.7b02724
Macromolecules 2018, 51, 3059−3065

imbibition time of ~120 s. Subsequently, the imbibition height was determined from cross sections by reflection microscopy (Zeiss Axiotech vario). Several cross sections were examined at each time that revealed uniformity in capillary imbibition. In addition, for each cross section imbibition heights at 10 different positions were recorded, at each imbibition time (the uncertainties are presented as error bars in Figures 4 and 6).

Rheology. The viscosities of the two homopolymers and their mixtures were measured by a shear rheometer (ARES). Measurements were made with the environmental test chamber as a function of temperature. Samples were prepared on the lower plate of a 13 mm diameter parallel plate geometry. The upper plate was brought into contact, the gap thickness was adjusted, and the sample was cooled. The storage (G') and loss (G'') shear moduli were monitored in different types of experiments. The linear and nonlinear viscoelastic ranges were identified from strain sweep experiments by recording the strain amplitude dependence of the complex shear modulus $|G^*|$ at selected temperatures. In subsequent experiments, frequency sweeps were performed at selected temperatures with strain amplitudes that correspond well within the linear viscoelastic range. The complex viscosity follows as $\eta^* = G''/\omega - iG'/\omega$, where ω is the angular velocity (in rad/s). Results for the viscosity of the homopolymers and their mixtures, all measured at 85 °C, are shown in Figure 1. The extracted zero-shear viscosity values (η_0) are included in Table 1.

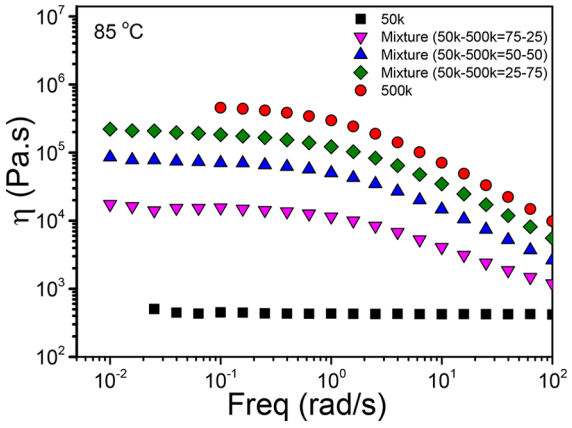

Figure 1. Measured viscosities for the two PEO homopolymers and their mixtures at 85 °C as a function of frequency.

Table 1. Parameters Employed by the LWE, Measured at 85 °C

sample	PEO 50k/ PEO 500k	γ ($\times 10^{-3}$ N/m)	θ_e (deg)	η_0 (Pa·s)
PEO 50k	1	29.1 ± 0.1	44 ± 1	(4.3 ± 0.1) × 10^2
PEO 500k	0	28.1 ± 0.1	41 ± 1	(4.6 ± 0.2) × 10^5
S1	75/25	28.9	42 ± 1	1.7 × 10^4
S2	50/50	28.6	42 ± 1	8.5 × 10^4
S3	25/75	28.4	42 ± 1	2.2 × 10^5

Surface Tension. Surface tension of the homopolymers was measured by the Wilhelmy plate method using a tension meter (DCAT 11BC, Dataphysics). Values for the two homopolymers were in close proximity, and the blend surface tension was obtained by a linear interpolation.

Contact Angle. To measure advancing contact angles of the homopolymers and their mixtures, we first formed spherical particles of 1 mm diameter by placing around 1 mg of sample on a soot-templated superamphiphobic surface at 85 °C for 96 h under vacuum.[12] Subsequently, the polymer sphere was slowly cooled below the melting temperature and transferred onto an electropolished Al disk coated by a thin native oxide layer. The latter comprises a flat model surface that mimics the AAO inner pore surface. Measurements of the advancing contact angles during spreading onto the substrate at 85 °C were made with a commercial goniometer (OCA35, Dataphysics).[13] While spreading, the contact angle was monitored as a function of time. A video showing the spreading of droplets corresponding to the homopolymers and their symmetric mixture is given in the Supporting Information. In general, contact angles of highly viscous homopolymers need long times to equilibrate. Dynamic contact angles depend on the velocity of the three-phase contact line. To estimate the "static" advancing contact angles (θ_e), measurements of the dynamic contact angles were extrapolated to zero velocity (Figure 2). The thus-obtained

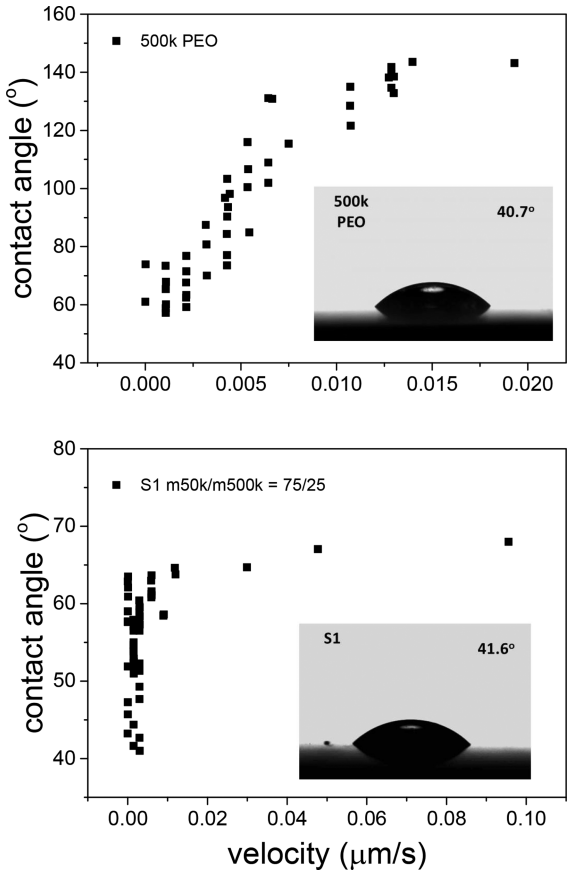

Figure 2. Dynamic contact angles of the homopolymer PEO 500k (top) and the symmetric SI mixture (bottom). The quasi-static advancing contact angles were estimated from the images shown as insets that correspond to the lowest contact line velocity measurements.

values are included in Table 1. The effect of employing the dynamic contact angle (DCA), θ_d, instead of the equilibrium one (ECA), θ_e, in the LWE is tested in Figure S2 of the Supporting Information for three different PEO homopolymers, by assuming $v = dH/dt$. Since $\theta_e > \theta_d$, the modified LWE invariably predicts a smaller capillary rise. Differences from the usual LWE are minor.

Gel Permeation Chromatography (GPC). The molecular weight distribution of the polymers located within AAO nanopores was measured with gel permeation chromatography (GPC) (Agilent Technologies 1260 infinity). Following imbibition at 85 °C for 11 h, the surface polymer was totally removed, and the polymer located within the nanopores was dissolved in chloroform. DMF was the eluent with elution rate of 1 mL/min at 60 °C. The samples were eluted through three SDV columns with a particle size of 10 μm and pore sizes of 10^6, 10^4, and 500 Å. UV−vis S-3702 (Soma) and DRI Shodex RI-101 (ECR) were used as detectors. Calibration was made using PEO standards provided by Polymer Standards Service.

3. COMPUTATIONAL DETAILS

Self-Consistent Field Theory. Self-consistent field theory (SCFT) for blends of homopolymer A or B (in bulk and in confinement) is based on the grand canonical ensemble.[13−19]

DOI: 10.1021/acs.macromol.7b02724
Macromolecules 2018, 51, 3059−3065

Briefly, each polymer is built from N_α monomers of species α = A, B. We use the homopolymer A as the reference and write $N_A = \kappa_A N$ with $\kappa_A = 1$. Polymers have the same associated Kuhn length, $b_A = b_B = b$. The monomers are assumed to have the same monomer density ρ_0. The average concentration is given by $\varphi_\alpha = n_\alpha \kappa_\alpha N/\rho_0 V$, where n_α is the total number of α-chains. We scale all lengths by the end-to-end distance of a Gaussian chain $R_e = b\sqrt{N}$, and the chain arc length by the degree of polymerization N. For simplicity, we assume short-range interactions of Flory–Huggins type, i.e., $\chi = \chi_{AB}$.

A/B Binary Blends in the Bulk. In the grand canonical ensemble, the controlling parameter is the chemical potential, μ_A and μ_B. As for the absolute energy scale we can set $\mu_A = 0$. The chemical potential can also be expressed in terms of activities as $z_A = \exp(\mu_A)/\kappa_A = 1/\kappa_A$ and $z_B = \exp(\mu_B)/\kappa_B$. The mean-field equations for A/B binary blends are

$$\begin{aligned} \varphi_A(\mathbf{r}) &= z_A \int_0^{\kappa_A} \mathrm{d}s\, q_A(\mathbf{r}, s) q_A(\mathbf{r}, \kappa_A - s) \\ \varphi_B(\mathbf{r}) &= z_B \int_0^{\kappa_B} \mathrm{d}s\, q_B(\mathbf{r}, s) q_A(\mathbf{r}, \kappa_B - s) \\ \omega_\alpha(\mathbf{r}) &= \chi \mathrm{N} \varphi_\beta(\mathbf{r}) + \eta(\mathbf{r}) \end{aligned} \tag{1}$$

$\sum_{a=A,B} \varphi_\alpha(\mathbf{r}) = 1$ where $\omega_\alpha(\mathbf{r})$ is the mean field experienced by α-species, $\eta(\mathbf{r})$ is the Lagrangian multiplier to enforce the incompressibility, and $q_\alpha(\mathbf{r},s)$ is the end-integrated propagator. The end-integrated propagator $q_\alpha(\mathbf{r},s)$ is the solution of the modified diffusion equation in the mean field $\omega_\alpha(\mathbf{r})$

$$\frac{\partial}{\partial s} q_\alpha(\mathbf{r}, s) = \frac{Nb^2}{6} \nabla^2 q_\alpha(\mathbf{r}, s) - \omega_\alpha(\mathbf{r}) q_\alpha(\mathbf{r}, s) \tag{2}$$

with the initial condition $q_\alpha(\mathbf{r},0) = 1$. The single-chain partition functions Q_α for α = A or B is given by

$$Q_\alpha(\{\omega_\alpha\}) = \frac{1}{V} \int \mathrm{d}\mathbf{r}\, q_\alpha(\mathbf{r}, \kappa_\alpha) \tag{3}$$

The free energy density is given by

$$\begin{aligned} g(\{\varphi\}, \{\omega\}) = \frac{1}{V} \int \mathrm{d}\mathbf{r} \{\chi \mathrm{N} \varphi_A(\mathbf{r}) \varphi_B(\mathbf{r}) - \sum_\alpha \omega_\alpha(\mathbf{r}) \varphi_\alpha(\mathbf{r})\} \\ - z_A Q_A - z_B Q_B \end{aligned} \tag{4}$$

Homogeneous Phase. For the homogeneous phase all the concentrations and fields are constant. The propagators are easily obtained in this case as $q_\alpha = \exp(-\omega_\alpha s)$ and $Q_\alpha = \exp(-\omega_\alpha \kappa_\alpha)$. Hence, the mean-field equations now read

$$\begin{aligned} \varphi_A &= Q_A = \mathrm{e}^{-\omega_A \kappa_A} \rightarrow \omega_A \kappa_A = -\ln \varphi_A \\ \varphi_B &= \mathrm{e}^{\mu_B} Q_B = \mathrm{e}^{\mu_B} \mathrm{e}^{-\omega_B \kappa_B} \rightarrow \omega_B \kappa_B = \mu_B - \ln \varphi_B \\ \omega_\alpha &= \chi \mathrm{N} \varphi_\beta + \eta \\ \sum_a \varphi_\alpha &= 1 \end{aligned} \tag{5}$$

The chemical potential μ_B is related to φ_α by

$$-\frac{\mu_B}{\kappa_B} = \chi \mathrm{N}(\varphi_B - \varphi_A) + \frac{\ln \varphi_A}{\kappa_A} - \frac{\ln \varphi_B}{\kappa_B} \tag{6}$$

Equation 6 is used to obtain the chemical potential, μ_B, from the bulk compositions φ_A and φ_B. The chemical potential, μ_B, is then used as an input parameter in the calculation of the cylindrical confinement. The free energy density for the bulk phase can be written in terms of φ_A:

$$g = \chi \mathrm{N} \varphi_B^2 + \frac{\ln \varphi_A}{\kappa_A} - \frac{\varphi_A}{\kappa_B} - \frac{\varphi_B}{\kappa_B} \tag{7}$$

A/B Binary Blends under Confinement. In the general SCFT framework, the total monomer density is unform everywhere $\varphi_0(r) = \varphi_A(r) + \varphi_B(r) = 1$. Under confinement, the hard surface is impenetrable, and the total monomer density has to vanish at the surface. A common method to solve this problem is to use a profile $\varphi_0(r)$ that decreases continuously from 1 to 0 in the proximity of the surface. For the detailed form of $\varphi_0(r)$, we use the one proposed by Meng and Wang.[20] In the cylindrical coordinates

$$\varphi_0(\mathbf{r}) = \begin{cases} 1 & r < R - \tau \\ \tanh^2\left[\dfrac{2\tau(R-\tau)}{\tau^2 - (R-r)^2}\right] & R - \tau < r < R \end{cases} \tag{8}$$

where R is the radius of the cylindrical pore and τ is the characteristic length of the surface layer (Figure 3).

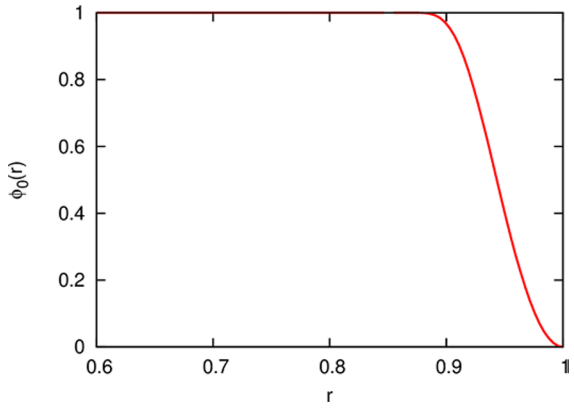

Figure 3. Total density profile near the hard wall. The characteristic length of the surface layer is $\tau = 0.15b\sqrt{N}$.

4. RESULTS AND DISCUSSION

Homopolymers. In general, for the homopolymers, the $t^{1/2}$ dependence is approximately valid.[6] Capillary rise in nanopores has been discussed in terms of the classical LWE[7,8,21−23] applicable to Newtonian liquids penetrating a cylindrical capillary of radius R:

$$h(t) = \left(\frac{\gamma R \cos\theta}{2\eta}\right)^{1/2} \sqrt{t} \tag{9}$$

Here, $h(t)$ is the penetration length of the liquid meniscus, γ is the surface tension, θ is the advancing contact angle, η is the viscosity, and t is the wetting time. The term $\cos\theta$ makes penetrability a function of the nature of the material comprising the capillary. Thus, both γ and $\cos\theta$ need to be evaluated separately for each polymer on the same surface. Furthermore, different from Newtonian liquids one has to take into account that the contact angle depends on wetting speed. In the calculation of the theoretical imbibition length, h, the measured respective parameters for the PEO 50k and PEO 500k homopolymers were employed (Table 1). However, the experimental

DOI: 10.1021/acs.macromol.7b02724
Macromolecules 2018, 51, 3059−3065

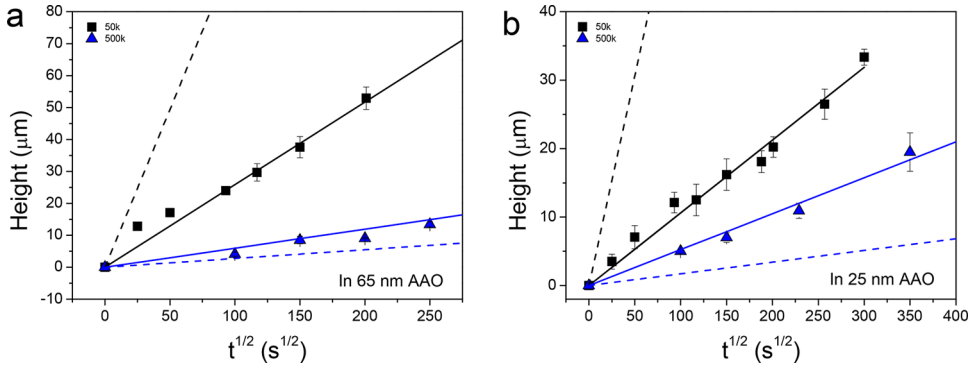

Figure 4. Imbibition heights as a fucntion of $t^{1/2}$ for the PEO homopolymers. Dashed lines give the predictions of the theoretical LWE for the PEO 50k (black) and PEO 500k (blue) within AAO templates with diameters of 65 nm (a) and 25 nm (b). Note the slower (faster) imbibition for the shorter (longer) chains as compared to the theoretical predictions by the LWE.

results for the homopolymers deviate substantially from the LWE predictions (Figure 4). For PEO 50k there is a slower capillary rise than theoretically predicted as opposed to chains with more entanglements (PEO 500k) that display a faster capillary rise. Results for other molecular weights and pore diameters were reported earlier.[6] The results demonstrate the breakdown of the LWE for non-Newtonian liquids (additional data are provided in Figure S3, for another pore diameter for the two homopolymers and their blends).

These results on the dynamics of polymer imbibition under nanometer confinement can be discussed by the combination of two mechanisms: The first is the standard hydrodynamic flow, resulting in a parabolic flow profile. In the situation when the inner wall has a strong attraction to the polymer chains, a layer of immobile chains (called "dead zone") is created. In this case we define an effective radius as $R_{eff} = R - \Delta R$, where ΔR is the thickness of the dead zone. The flow velocity is given by

$$v_{flow} = \frac{R_{eff}^2}{8\eta_0 h}\frac{2\gamma \cos\theta}{R} \tag{10}$$

Since only the R_{eff}^2/R^2 portion of the polymer contributes to the flow

$$\dot{h} = v_{flow}\frac{R_{eff}^2}{R^2} = \frac{\gamma \cos\theta R_{eff}^4}{4\eta_0 h R^3} \tag{11}$$

This dead zone reduces the effective pore radius, leading to an increase of the effective viscosity.

The second mechanism is based on the reptation model, proposed earlier by Johner et al.[5] According to the model, material transport is achieved mainly by the reptation of free polymer chains in the network driven by the pressure gradient. Each free polymer feels a force

$$[-p(x + R_x) + p(x)]l^2 = -l^2 R_x \frac{dp}{dx} \tag{12}$$

where l^2 is the cross section and R_x is the end-to-end vector along the pore axis. The polymer velocity along the tube is

$$v_c = -\frac{l^2}{\zeta N} R_x \frac{dp}{dx} \tag{13}$$

where ζ is the friction constant for one Kuhn segment. The averaged velocity of the center of mass of the polymer is

$$v_g = \frac{R_x}{L} v_c = -\frac{l^2}{\zeta N L} R_x^2 \frac{dp}{dx} = -\frac{l^2 a_t}{3\zeta N}\frac{dp}{dx} \tag{14}$$

where L is the contour length of the tube, given by $L = (N/N_e)a_t$, N_e is the entanglement length, and $a_t = \sqrt{N_e}\,b$ is the tube diameter. Moreover, R_x^2 is assumed to be ideal, i.e., $R_x^2 = Nb^2/3$. The filling speed is then given by

$$\dot{h} = \varphi v_g = \varphi \frac{l^2 a_t}{3\zeta N}\frac{2\gamma \cos\theta}{hR} \tag{15}$$

where φ is the fraction of free polymers. This mechanism leads to a decrease of the effective viscosity. By varying the pore radius from large to small, initially the hydrodynamic mode dominates and the effective viscosity increases. As the pore radius gets smaller, the reptation mechanism takes over, and the effective viscosity starts to decrease. Experiments have shown that the critical pore radius corresponding to the transition depends on the polymer molecular weight.[6] For shorter chains, the experiment revealed the nonmonotonic behavior of the effective viscosity. For longer chains, on the other hand, the critical radius is very small, and only the decrease of the effective viscosity was observed. Overall, the competition between the two mechanisms has as a result the reversal in the imbibition mechanism with increasing polymer molecular weight.[24]

Other effects that can influence the capillary imbibition are the surface roughness and the change of the liquid-to-glass temperature (T_g) at the surface. With respect to the surface roughness, recently we evaluated the internal pore surface roughness of AAO by atomic force microscopy.[25] It was found to be ≤0.6 nm, i.e., of the order of the statistical segment length for PEO. Under conditions that the statistical segment length is smaller than the AAO surface roughness certain repeat units can be entrapped within the corrugated surface and slow down capillary rise. On the other hand, the changes in the T_g cannot account for the large changes in the effective viscosity under confinement. It was recently documented that there is a trend for a decreasing glass temperature relative to the bulk with increasing interfacial energy for polymers located inside AAO nanopores.[26] However, for PEO the reduction of the glass temperature (~6 K) brings a decrease in viscosity of only 15% that cannot account for the experimental findings. We now turn our attention to the blend imbibition process.

Polymer Mixtures. Representative reflection microscopy images of the capillary imbibition process for the three blend compositions are depicted in Figure 5. Images show the rise of the imbibition front within the AAO capillaries with time. Notably the imbibition times are very slow for polymers, but this is only

DOI: 10.1021/acs.macromol.7b02724
Macromolecules 2018, 51, 3059−3065

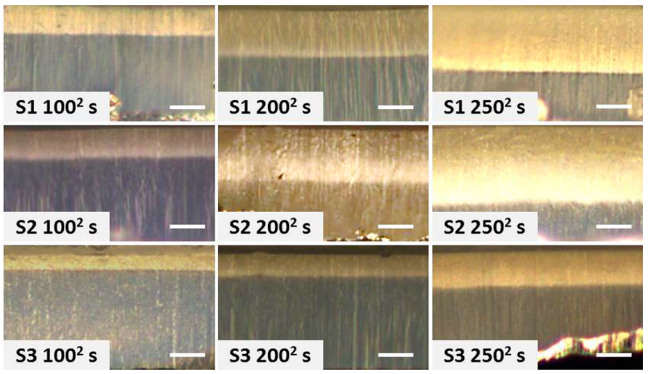

Figure 5. Reflection microscope images of PEO mixtures located inside 65 nm AAO infiltrated for different times: (top) S1 (PEO 50k/PEO 500k = 75/25); (middle) S2 (50k/500k = 50/50); (bottom): S3 (50k/500k = 25/75). Scale bar indicates 20 μm. (Times are shown as 100^2, 200^2, and 250^2 s that correspond to approximately 2.8, 11.1, and 17.4 h, respectively.)

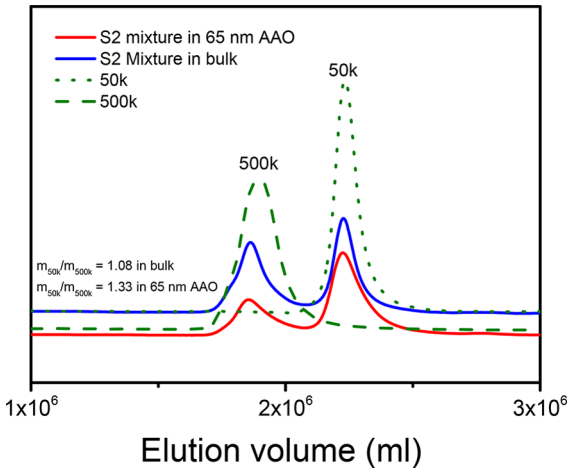

Figure 7. GPC traces of S2 symmetric mixture within AAO pores with a diameter of 65 nm (red line) compared with the same mixture in the bulk (blue line) and with the two homopolymers PEO 50k and PEO 500k. The mass ratio of PEO 50k to PEO 500k was obtained from the integration of the corresponding peaks.

partially due to the bulk viscosity.[6] The results with respect to the imbibition length, h, as a function of $t^{1/2}$ are summarized in Figure 6 (additional data in Figure S2).

In the binary mixtures, the imbibition lengths follow approximate $t^{1/2}$ dependence in accord with the LWE. However, theoretical imbibition lengths, which are based on the measured viscosities (Figure 1), the measured quasi-static advancing contact angles (Figure 2 and Supporting Information), and the surface tensions (Table 1), deviate strongly from the experimental values. Hence, the LWE breaks down as with the homopolymers (Figure 4). In addition, imbibition lengths are biased toward the PEO 50k homopolymer (i.e., the shorter chains) (Figure 6 and Figure S3). This is evident for all blend compositions and both AAO pore diameters. For example, AAO pores with diameter of 65 nm are enriched by 20% in shorter chains. AAO templates with a pore diameter of 25 nm are enriched by ~10% in shorter chains. To further explore this effect, GPC was made on material extracted from the AAO pore interior. The result is presented in Figure 7 and confirms an enrichment of the pores by the shorter chains.

With self-consistent field theory (SCFT)[14−20] we study a blend of the same chemical composition (i.e., $\chi = 0$) and length ratio $\alpha = 10$. As with the experiments we consider three bulk compositions (A and B denote the polymer with the short and long chains, respectively) as follows: (i) $\varphi_A = 0.25$, $\varphi_B = 0.75$; (ii) $\varphi_A = \varphi_B = 0.50$; and (iii) $\varphi_A = 0.75$, $\varphi_B = 0.25$. The cylinder radius is varied from $0.5b\sqrt{N}$ to $8.0b\sqrt{N}$. Figure 8 summarizes the pertinent results of the numerical calculations. In general, shorter chains more easily penetrate the pores, and the effect becomes more pronounced with increasing degree of confinement ($R \rightarrow 0$). These results from SCFT calculations are in excellent agreement with experiment. For the symmetric blend located inside AAO with a pore diameter ($2R$) of 65 nm, the individual components have end-to-end distances of $1.7R$ (PEO 50k) and $0.57R$ (PEO 500k), suggesting on average an ~15% enrichment by the shorter chains. On the other hand, in the limit of increasing R, the bulk ratio is approached.

Subsequently, we study the density profiles inside the pore for a given pore radius ($R = 0.5b\sqrt{N}$). The second row of Figure 8 depicts the spatial distribution of polymer chains as a function of r, the distance to the pore axis. In all cases the inner part of the pores is enriched by the shorter chains. For example, for the symmetric blend, the composition near the pore center is 55:45, and this persists to $r = 0.4b\sqrt{N}$. The local density ratio between the short and long chains is also of interest

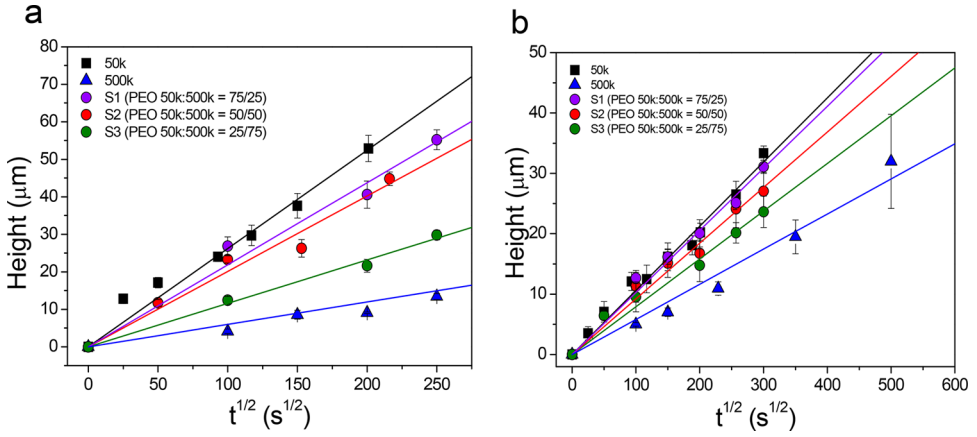

Figure 6. Imbibition length, h, as a function of $t^{1/2}$ for two PEO homopolymers with molecular weights of 50k (squares) with 500k (triangles) and their mixtures with compositions: 50/50 (red spheres), 75/25 (magenta spheres), and 25/75 (green spheres) located inside AAO with pore diameters of (a) 65 nm and (b) 25 nm. Lines represent the result of a linear fit to the homopolymers and their mixtures.

DOI: 10.1021/acs.macromol.7b02724
Macromolecules 2018, 51, 3059−3065

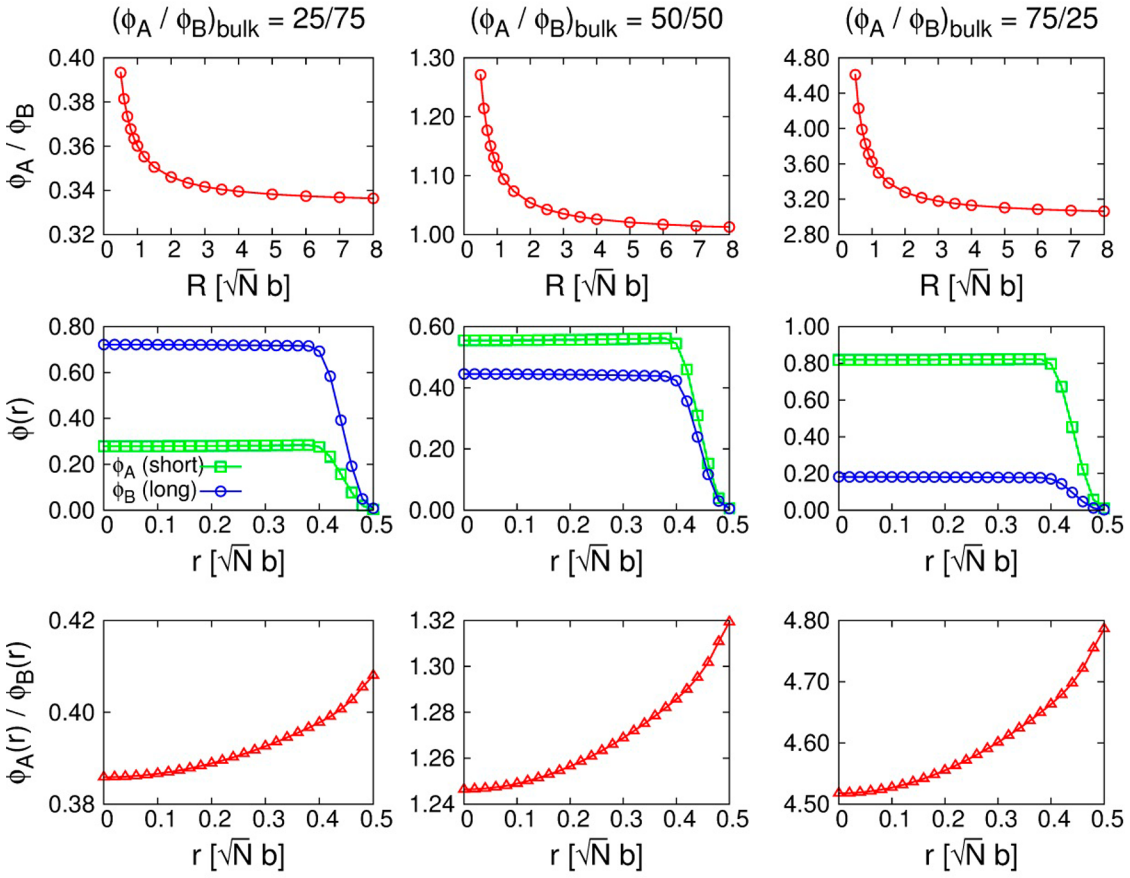

Figure 8. Self-consistent field theory calculations for three blend composisions: (left column) $\varphi_A = 0.25$, $\varphi_B = 0.75$; (middle column) $\varphi_A = \varphi_B = 0.50$; and (right column) $\varphi_A = 0.75$, $\varphi_B = 0.25$. The results of the averaged φ_A/φ_B is shown in the first row as a fucntion of the cylinder radius R (in units of $b\sqrt{N}$). The spatial distribution of the polymers as a fucntion of r, the distance to the pore axis is shown in the second row. The local density ratio of short to long chains is plotted in the third row.

(third row of Figure 8). From an entropic point of view, ends of polymer chains have equal probability to be found near the pore surface. Consequently, there is an enrichment of the short chains near the pore surface.

Overall, SCFT calculations confirmed the faster imbibition of nanopores by the shorter chains. Furthermore, they suggest the enrichment of the pore surface by the shorter chains. The importance of these findings is that they suggest a way of separating long from short chains in a polydisperse polymer mixture that is based on the difference in their imbibition speeds. A careful selection of the pore diameter relative to the polymer molecular weight can lead to the *fractionation* of a polydisperse melt in the absence of solvent.

5. CONCLUSION

In summary, capillary imbibition in binary blends follows approximately $t^{1/2}$ dependence but contradicts the predictions of the classical LWE because of the prefactor in the equation. Results from reflection microscopy demonstrate faster imbibition by the shorter chains. Results from SCFT calculations, performed on the same mixtures, are in excellent agreement with experiment, suggesting on average an ~15% enrichment by the shorter chains. On top of that, SCFT shows an enrichment of the short chains near the pore surface. These results taken together suggest a way of separating long from short polymer chains in the bulk, namely, by the difference in imbibition speeds within narrow pores. Whereas in gel permeation chromatography (GPC) smaller polymer coils explore more pores and thus take longer to pass through a GPC column, in AAO, shorter chains penetrate faster purely for entropic reasons and in the absence of solvent.

■ ASSOCIATED CONTENT

Supporting Information

The Supporting Information is available free of charge on the ACS Publications website at DOI: 10.1021/acs.macromol.7b02724.

Discussion of the dynamic contact angle as well as additional reflection microscopy data for another pore diameter (35 nm); Figures S1−S3 (PDF)

Video of spreading of droplets corresponding to the two homopolymers and their symmetric mixture (AVI)

■ ACKNOWLEDGMENTS

We are thankful to Prof. M. Steinhart for AAO nanopores and polished alumina surface and to Dr. S. Wooh for soot-templated superamphiphobic surface. We also thank A. Best and A. Hanewald for help with reflection microscopy and rheology, respectively.

■ AUTHOR INFORMATION

Corresponding Authors

*E-mail gfloudas@uoi.gr (G.F.).
*E-mail jjzhou@buaa.edu.cn (J.Z.).

DOI: 10.1021/acs.macromol.7b02724
Macromolecules 2018, 51, 3059−3065

ORCID

Hans-Juergen Butt: 0000-0001-5391-2618
Jiajia Zhou: 0000-0002-2258-6757
George Floudas: 0000-0003-4629-3817

Notes

The authors declare no competing financial interest.

REFERENCES

(1) de Gennes, P. G. *Scaling Concepts in Polymer Physics*; Cornell University Press: 1979.
(2) Movileanu, L.; Cheley, S.; Bayley, H. Partitioning of individual flexible polymers into a nanoscopic protein pore. *Biophys. J.* **2003**, *85*, 897−910.
(3) Aksimentiev, A.; Heng, J. B.; Timp, G.; Schulten, K. Microscopic kinetics of DNA translocation through synthetic nanopores. *Biophys. J.* **2004**, *87*, 2086−2097.
(4) Shin, K.; Obukhov, S.; Chen, J.-T.; Huh, J.; Hwang, Y.; Mok, S.; Dobriyal, P.; Thiyagarajan, P.; Russell, T. P. Enhanced mobility of confined polymers. *Nat. Mater.* **2007**, *6*, 961−965.
(5) Johner, A.; Shin, K.; Obukhov, S. Nanofluidity of a polymer melt: Breakdown of poiseuille's flow model. *Europhys. Lett.* **2010**, *91*, 38002.
(6) Yao, Y.; Alexandris, S.; Henrich, F.; Auernhammer, G.; Steinhart, M.; Butt, H.-J.; Floudas, G. Complex dynamics of capillary imbibition of poly(ethylene oxide) melts in nanoporous alumina. *J. Chem. Phys.* **2017**, *146*, 203320.
(7) Lucas, R. Ueber das zeitgesetz des kapillaren aufstiegs von flüssigkeiten,. *Colloid Polym. Sci.* **1918**, *23*, 15−22.
(8) Washburn, E. W. The dynamics of capillary flow. *Phys. Rev.* **1921**, *17*, 273−283.
(9) Masuda, H.; Fukuda, K. Ordered metal nanohole arrays made by a two-step replication of honeycomb structures of anodic alumina. *Science* **1995**, *268* (5216), 1466.
(10) Masuda, H.; Hasegwa, F.; Ono, S. Self-Ordering of Cell Arrangement of Anodic Porous Alumina Formed in Sulfuric Acid Solution. *J. Electrochem. Soc.* **1997**, *144* (5), L127−L130.
(11) Masuda, H.; Yada, K.; Osaka, A. Self-ordering of cell configuration of anodic porous alumina with large-size pores in phosphoric acid solution. *Jpn. J. Appl. Phys.* **1998**, *37* (11A), L1340.
(12) Deng, X.; Mammen, L.; Butt, H.-J.; Vollmer, D. Candle soot as a template for a transparent robust superamphiphobic coating. *Science* **2012**, *335*, 67−70.
(13) See Supporting Information Figure S1 for a video of the advancing contact angle during spreading of the homopolymers and the blend with the symmetric composition.
(14) Schmid, F. Self-consistent-field theories for complex fluids. *J. Phys.: Condens. Matter* **1998**, *10*, 8105.
(15) Matsen, M. W. The standard Gaussian model for block copolymer melts,. *J. Phys.: Condens. Matter* **2002**, *14*, R21.
(16) Shi, A.-C. Self-Consistent Field Theory of Block Copolymers. In *Developments in Block Copolymer Science and Technology*; Hamley, I. W., Ed.; John Wiley & Sons: New York, 2004; Chapter 8.
(17) Fleer, G. J.; Cohen Stuart, M. A.; Scheutjens, J. M. H. M.; Cosgrove, T.; Vincent, B. *Polymer at Interfaces*; Chapman & Hall: London, 1993.
(18) Kawakatsu, T. *Statistical Physics of Polymers*; Springer: Berlin, 2004.
(19) Fredrickson, G. H. *The Equilibrium Theory of Inhomogeneous Polymers*; Clarendon Press: Oxford, 2006.
(20) Meng, D.; Wang, Q. Hard-surface effects in polymer self-consistent field calculations. *J. Chem. Phys.* **2007**, *126*, 234902.
(21) Dimitrov, D. I.; Milchev, A.; Binder, K. Capillary rise in nanopores: Molecular dynamics evidence for the Lucas-Wahburn equation. *Phys. Rev. Lett.* **2007**, *99*, 054501.
(22) Stukan, M. R.; Ligneul, P.; Crawshaw, J. P.; Boek, E. S. Spontaneous imbibition in naopores of different roughness and wettability. *Langmuir* **2010**, *26*, 13342−13352.
(23) Stroberg, W.; Keten, S.; Liu, W. K. Hydrodynamics of capillary imbibition under nanoconfinement. *Langmuir* **2012**, *28*, 14488−14495.
(24) Yao, Y.; Butt, H.-J.; Floudas, G.; Zhou, J.; Doi, M. Theory on capillary filling of polymer melts in nanopores. *Macromol. Rapid Commun*, accepted, 2018.
(25) Suzuki, Y.; Steinhart, M.; Kappl, M.; Butt, H.-J.; Floudas, G. Effects of polydispersity, additives, impurities and surfaces on the crystallization of poly(ethylene oxide)(PEO) confined to nanoporous alumina. *Polymer* **2016**, *99*, 273−280.
(26) Alexandris, S.; Papadopoulos, P.; Sakellariou, G.; Steinhart, M.; Butt, H.-J.; Floudas, G. Interfacial Energy and Glass Temperature of Polymers Confined to Nanoporous Alumina. *Macromolecules* **2016**, *49* (19), 7400−7414.

DOI: 10.1021/acs.macromol.7b02724
Macromolecules 2018, 51, 3059−3065